

Square-lattice Heisenberg antiferromagnet with two kinds of nearest-neighbor regular bonds

N. B. Ivanov

*Institute for Solid State Physics, Bulgarian Academy of Sciences,
Tzarigradsko chaussee-72, 1784 Sofia, Bulgaria*

S. E. Krüger and J. Richter

*Institut für Theoretische Physik, Universität Magdeburg,
P.O.Box 4120, D-39016 Magdeburg, Germany*

(June 28, 2021)

We study the zero-temperature phase diagram of a square-lattice $S = 1/2$ Heisenberg antiferromagnet with two types of regularly distributed nearest-neighbor exchange constants, $J_1 > 0$ (antiferromagnetic) and $-\infty < J_2 < \infty$, using spin-wave series based on appropriate mean-field Hamiltonian and exact-diagonalization data for small clusters. At a quasiclassical level, the model displays two critical points separating the Néel state from (i) a helicoidal magnetic phase for relatively small frustrating ferromagnetic couplings $J_2 < 0$ ($J_2/J_1 < -1/3$ for classical spins), and (ii) a finite-gap quantum paramagnetic phase for large enough antiferromagnetic exchange constants $J_2 > 0$. The quantum order-disorder transition (ii) is similar to the one recently studied in two-layer Heisenberg antiferromagnets and is a pure result of the zero-point spin fluctuations. On the other hand, the melting of the Néel state in the ferromagnetic region, $J_2 < 0$, is a combined effect of the frustration and quantum spin fluctuations. The second-order spin-wave calculations of the ground-state energy and on-site magnetization are in accord with our exact diagonalization data in a range away from the quantum paramagnetic phase. In approaching the phase boundary, the theory fails due to the enhanced longitudinal spin fluctuations, as it has recently been argued by Chubukov and Morr.

PACS: 75.50.Ee, 75.10.Jm, 75.30.Kz, 75.10.-b

I. INTRODUCTION

The zero-temperature properties of a number of two-dimensional Heisenberg spin models displaying order-disorder quantum phase transitions have recently attracted much attention. Most efforts were connected with the square-lattice Heisenberg antiferromagnets with frustrating second J_2 and third J_3 nearest-neighbor bonds¹ as well as with the two-layer quantum Heisenberg models².

The mentioned models present concrete realizations of the quantum order-disorder transition considered by Chakravarty, Halperin, and Nelson³ using a macroscopical approach based on the quantum non-linear σ model in $2+1$ dimensions. Notice that in the $J_1 - J_2 - J_3$ models the destruction of the Néel state is a result of both the frustration and zero-point spin fluctuations, whereas the two-layer antiferromagnet can be turned through an order-disorder transition by varying the antiferromagnetic exchange coupling between the planes. The latter model constitutes an ideal system where the zero-point spin fluctuations destroy the classical Néel state.

Less studied are the $2D$ Heisenberg antiferromagnets with random ferromagnetic exchange bonds⁴ which are currently considered as an appropriate model of the copper-oxygen sheets of lightly doped insulating high- T_c superconductors. The idea comes from Aharony and co-workers⁵ who suggested that the holes introduced into the CuO layers are localized at individual oxygen sites. The coupling between the copper and oxygen spins results in an effective ferromagnetic coupling between the copper spins situated near an oxygen.

In this paper we study a quantum Heisenberg antiferromagnet with two kinds of nearest-neighbor exchange couplings, regularly distributed on the square lattice, Fig.1. The relevance of the model is twofold. First, it combines the features of the $J_1 - J_2 - J_3$ and two-layer models in displaying the mentioned two mechanisms of destruction of the Néel phase and, on the other hand, the model can be considered as a prototype of some more realistic antiferromagnetic models containing ferromagnetic bonds.

The Hamiltonian of the system reads

$$H = J_1 H_1 + J_2 H_2 \equiv J_1 \sum_{\langle ij \rangle} \mathbf{S}_i \mathbf{S}_j + J_2 \sum_{(ij)} \mathbf{S}_i \mathbf{S}_j, \quad (1)$$

where the sums run over the nearest-neighbor J_1 and J_2 bonds, respectively. In what follows we frequently use the notations $\alpha \equiv J_2/J_1$, $J_1 \equiv 1$. In the antiferromagnetic region $J_2 > 0$, Singh, Gelfand, and Huse⁶ have found for Eq.(1) a critical point $\alpha_s \approx 2.56$ separating the classical Néel ordered and a finite-gap quantum paramagnetic phases, using series expansions around the dimer Hamiltonian H_2 . They also argued that the critical exponents are consistent with those of the 3D classical Heisenberg model. In this study we analyze the zero-temperature phase diagram of the model in the range $-\infty < J_2 < \infty$ both analytically, reducing the problem to an interacting Bose gas, and numerically, throughout exact diagonalization of small clusters. For ferromagnetic exchange bonds, at $\alpha = -1/3$ for classical spins, we found another critical point, dividing the Néel phase from a helicoidal magnetic phase, Fig.1. The latter phase reduces to a three-sublattice Néel state in the limit $J_2 = -\infty$. The classical helicoidal phase is described by the equations

$$\begin{aligned} \mathbf{S}_A(\mathbf{R}) &= \hat{\mathbf{u}} \cos \mathbf{QR} + \hat{\mathbf{v}} \sin \mathbf{QR}, \\ \mathbf{S}_B(\mathbf{R} + \hat{\mathbf{x}}) &= \hat{\mathbf{u}} \cos(\mathbf{QR} + \pi + 3\Phi) + \hat{\mathbf{v}} \sin(\mathbf{QR} + \pi + 3\Phi), \end{aligned} \quad (2)$$

where the classical spins \mathbf{S}_A and \mathbf{S}_B belong to the sublattice A and B , respectively. $\hat{\mathbf{u}}$ and $\hat{\mathbf{v}}$ are perpendicular unit vectors in the spin space; \mathbf{R} runs over the sites of the sublattice A . The pitch vector \mathbf{Q} and the phase Φ are determined through the relations

$$\begin{aligned} \cos Q_{x(y)} &= \frac{1}{2} \left(\frac{1}{|\alpha|} - 1 \right), & Q_{y(x)} &= 0, \\ \Phi &= \frac{Q_{x(y)}}{2}, & \alpha &\leq -\frac{1}{3}. \end{aligned} \quad (3)$$

The angle Φ can be chosen as an order-parameter of the continuous classical transition.

Below we concentrate on an analysis of the role of quantum spin fluctuations in the Néel phase of Eq.(1). To this end, in the next section we follow a method overcoming the problems of the standard spin-wave theory (SWT) connected to logarithmic divergences at the classical transition points. Then we construct spin-wave series for the ground-state energy and on-site magnetization, and discuss the changes in the phase diagram implied by the interaction. In the last section we present exact diagonalization (ED) data for small clusters and compare them with the theory.

II. SPIN-WAVE SERIES FOR THE GROUND-STATE ENERGY AND ON-SITE MAGNETIZATION

We proceed with a short discussion of the results implied by the linear spin-wave theory (LSWT). LSWT predicts the existence of a region around the classical transition point $\alpha_c = -1/3$, where the magnetic states are completely melt by the zero-point spin fluctuations, Fig.2. In this approximation, the spin-liquid phase exists for arbitrary S due to the logarithmic divergence at $\alpha = -1/3$ in the integral

$$\delta m = \frac{1 - \kappa_0}{N} \sum_{\mathbf{k}} \frac{1}{\varepsilon_{s\mathbf{k}}} - \frac{1}{2} \sim \ln \frac{1}{|\alpha - \alpha_c|}, \quad (4)$$

defining the reduction of the on-site magnetization $\delta m = S - \langle S_z \rangle$. Here N is the number of lattice sites, $\kappa_0 = (1 - \alpha)/4$. This behavior of δm can be regarded as an aftereffect of the classical "soft lines" at the critical point in the low-energy magnon dispersion function

$$\varepsilon_{s\mathbf{k}} \sim \sqrt{c_1(\alpha - \alpha_c)k_x^2 + c_2k_y^2}, \quad |\mathbf{k}| \approx 0, \pi. \quad (5)$$

Due to the continuous character of the classical transition, one could expect the same behavior when the interaction is switched on. A consideration valid in the large- S limit, and based on an appropriate quantum nonlinear σ model on the critical line⁷, predicts the existence of a disordered spin-liquid phase in an exponentially small region around the critical line. There are some indications that the spin-liquid phase survives for arbitrary S up to the extreme quantum limit $S = 1/2$ ⁸. In our case, however, the structure of the quasiparticle spectrum (i.e., the number of Goldstone modes) is changed, so that the problem requires a special study⁹ of the helicoidal phase, which is beyond the scope of the present paper.

LSWT also qualitatively predicts the transition to a finite-gap quantum paramagnetic state in the antiferromagnetic, $J_2 > 0$, region of the phase diagram¹⁰. However, the estimate $\alpha_s \approx 10.6$ considerably exceeds the series estimate $\alpha_s \approx 2.56$. The situation is analogous to the one in two-layer antiferromagnets¹¹, i.e., SWT is not successful because of the enhanced longitudinal spin fluctuations. One of the purposes of the present study, using also exact diagonalization data, is to see to what extent SWT can be trust in approaching the quantum paramagnetic phase. Our model has the advantage of permitting exact diagonalization studies for large enough clusters.

A. The method

As mentioned above, the standard spin-wave series are divergent at the classical transition point $\alpha_c = -1/3$. For example, the first-order correction to the on-site magnetization $\Delta m^{(1)}$ is expressed through the following divergent integrals

$$\begin{aligned}\Delta m^{(1)} &= \frac{a_0}{S} \frac{1}{N} \sum_{\mathbf{k}} \frac{(\nu_{\mathbf{k}} - \kappa_0 \cos k_x)(\cos k_x - \nu_{\mathbf{k}}) - \kappa_0 \sin^2 k_x}{\varepsilon_{s\mathbf{k}}^3}, \\ a_0 &= -\frac{\kappa_0}{N} \sum_{\mathbf{k}} \frac{\kappa_0(1 - \nu_{\mathbf{k}} \cos k_x) + \nu_{\mathbf{k}}(\nu_{\mathbf{k}} - \cos k_x)}{\varepsilon_{s\mathbf{k}}},\end{aligned}\tag{6}$$

where $\nu_{\mathbf{k}} = (\cos k_x + \cos k_y)/2$, $\varepsilon_{s\mathbf{k}} = \sqrt{(1 - \nu_{\mathbf{k}}^2) - 2\kappa_0(1 - \nu_{\mathbf{k}} \cos k_x)}$. Since in the SWT formalism the on-site magnetization is a two-boson operator, it is clear that the divergences in the first-order correction $\Delta m^{(1)}$ come from two-boson interaction terms. A straightforward way to improve the situation is to use a normal-ordered operator form for the interaction. This approach leads to renormalization of the quasiparticle excitation spectrum and to some resummed SWT series starting now from an appropriate mean-field theory (MFT). Instead of $1/S$, the new series are, however, governed by a formal small parameter λ introduced in front of the quartic Dyson-Maleev normal-ordered boson interaction. Therefore, the quality of the series should be controlled through another method. In our study we present exact diagonalization data for small clusters.

Let us briefly describe the procedure leading to the spin-wave series. SWT requires three subsequent transformations. Through a standard Dyson-Maleev bosonization scheme, the original spin Hamiltonian transforms into equivalent boson Hamiltonian. In the usual SWT the two-boson terms scaling with S constitute the free-boson Hamiltonian H_0 which fixes the $1/S$ series. As it was mentioned above, in our case more convenient is to diagonalize the quadratic part of the Hamiltonian by means of a generalized Bogoliubov transformation, also touching on the anharmonic terms¹²⁻¹⁴. The new quadratic Hamiltonian H_0 can be obtained in the following way. First, we subsequently do the Fourier and quasiparticle Bogoliubov transformations, the latter being defined through the relations

$$a_{\mathbf{k}} = u_{\mathbf{k}}\alpha_{\mathbf{k}} + v_{\mathbf{k}}\beta_{\mathbf{k}}^{\dagger}, \quad b_{\mathbf{k}} = u_{\mathbf{k}}\beta_{\mathbf{k}} + v_{\mathbf{k}}\alpha_{\mathbf{k}}^{\dagger}, \quad |u_{\mathbf{k}}|^2 - |v_{\mathbf{k}}|^2 = 1.\tag{7}$$

In a quasiparticle representation, the boson Hamiltonian takes the form

$$H = E_0 + H_0 + V_{DM},\tag{8}$$

where the Dyson-Maleev interaction V_{DM} is in a normal-ordered operator form (see Appendix A). Then E_0 is the mean-field ground-state energy and H_0 is a quadratic free-particle Hamiltonian, containing also contributions from the operator ordering of the quartic interaction term.

The diagonalization of H_0 , which in terms of quasiparticle operators reads

$$H_0 = \sum_{\mathbf{k}} \left[E_{\mathbf{k}}(\alpha_{\mathbf{k}}^{\dagger}\alpha_{\mathbf{k}} + \beta_{\mathbf{k}}^{\dagger}\beta_{\mathbf{k}}) + (B_{\mathbf{k}}\alpha_{\mathbf{k}}^{\dagger}\beta_{\mathbf{k}}^{\dagger} + h.c.) \right],\tag{9}$$

requires $B_{\mathbf{k}} = 0$. In principle, the condition $B_{\mathbf{k}} = 0$ leads to some integral equations for $u_{\mathbf{k}}$ and $v_{\mathbf{k}}$ studied in the general case by Obukhov¹⁵. Recently, similar method has been applied to the $J_1 - J_2$ model¹⁶.

Note that the so-defined mean-field theory can also be regarded as a result of the variational equations

$$\frac{\delta \langle \Psi | H | \Psi \rangle}{\delta u_{\mathbf{k}}} = 0, \quad \frac{\delta \langle \Psi | H | \Psi \rangle}{\delta v_{\mathbf{k}}} = 0\tag{10}$$

(under the constraint $|u_{\mathbf{k}}|^2 - |v_{\mathbf{k}}|^2 = 1$), defining the generalized Bogoliubov transformation. The quality of the discussed perturbation scheme mainly depends on the quasiparticle interaction strength playing the role of a physical small parameter. Particularly, the latter is expected to increase near the critical points. The model Hamiltonian (1) represents a convenient system to check the theory due to the existing two critical points and a numerical-series estimate⁶ for the order-disorder transition point.

B. Zeroth-order mean-field approximation

The above program is straightforward for Eq.(1) and leads to a renormalization of the bare coupling $(1 - J_2/J_1) \rightarrow (1 - J_2/J_1)Z$. The implicit equation for the factor $Z = Z(S, \alpha)$ reads

$$Z = \frac{S - a_1}{S - a_2}, \quad (11)$$

where

$$a_1 = -\frac{1}{2} + \frac{1}{N} \sum_{\mathbf{k}} \frac{1 - \nu_{\mathbf{k}} \cos k_x}{\varepsilon_{\mathbf{k}}}, \quad a_2 = -\frac{1}{2}(1 - \kappa) + \kappa a_1 + \frac{1}{N} \sum_{\mathbf{k}} \varepsilon_{\mathbf{k}}, \quad (12)$$

$$\varepsilon_{\mathbf{k}} = \sqrt{(1 - \nu_{\mathbf{k}}^2) - 2\kappa(1 - \nu_{\mathbf{k}} \cos k_x)}, \quad \kappa = (1 - \alpha) \frac{Z}{4}. \quad (13)$$

The renormalization factor Z defines (up to an irrelevant phase factor) the Bogoliubov coefficients $u_{\mathbf{k}}$ and $x_{\mathbf{k}} = -v_{\mathbf{k}}/u_{\mathbf{k}}$

$$\begin{aligned} u_{\mathbf{k}} &= \sqrt{\frac{1 - \kappa + \varepsilon_{\mathbf{k}}}{2\varepsilon_{\mathbf{k}}}} \\ \Re(x_{\mathbf{k}}) &= \frac{\nu_{\mathbf{k}} - \kappa \cos k_x}{(1 - \kappa + \varepsilon_{\mathbf{k}})}, \\ \Im(x_{\mathbf{k}}) &= \frac{-\kappa \sin k_x}{(1 - \kappa + \varepsilon_{\mathbf{k}})}, \end{aligned} \quad (14)$$

Notice that one cannot choose the phase factor so as to make both $u_{\mathbf{k}}$ and $v_{\mathbf{k}}$ real functions.

The quasiparticle excitation spectrum reads

$$E_{\mathbf{k}} = 4S \left(1 + \frac{r}{2S}\right) \varepsilon_{\mathbf{k}}, \quad (15)$$

where r is a numerical factor analogous to Oguchi's correction¹⁷, $r = -2a_2$.

The ground-state energy E_0 and on-site magnetization m_0 in this approximation are

$$\frac{E_0}{2N} = -(1 - \kappa Z)(S - a_2)^2, \quad (16)$$

$$m_0 = S + \frac{1}{2} - \frac{1 - \kappa}{N} \sum_{\mathbf{k}} \frac{1}{\varepsilon_{\mathbf{k}}}. \quad (17)$$

We will see below that the mean-field estimate for the ground-state energy E_0 is in agreement with ED in a large region of the phase diagram. The on-site magnetization m_0 vanishes at $\alpha_c \approx -3.0$, i.e., there is a shift of the classical transition point towards the helicoidal phase. This phenomenon is known as "Villain's order from disorder"¹⁸. The transition to quantum paramagnetic state in MFT is located at $\alpha_s \approx 5.7$, which is approximately twice larger than the series estimate. Below we show that the second-order correction to this result improves the estimate.

C. Second-order corrections to E_0 and m_0

Now we proceed with a calculation of the second-order $O(V_{DM}^2)$ corrections to E_0 and m_0 . It is easy to see that the first-order corrections both to E_0 and m_0 identically vanish for the normal-ordered interaction V_{DM} . The second-order correction to E_0 has the standard form (Appendix B)

$$\frac{\Delta E^{(2)}}{2N} = -\left(\frac{2}{N}\right)^3 \sum_{1-4} \Delta(1+2-3-4) \frac{V^{(7)}(1234)V^{(8)}(3412)}{E_1 + E_2 + E_3 + E_4}, \quad (18)$$

where $E_{\mathbf{k}}$ are the quasiparticle energies Eq.(15). The expression for the second-order correction to the on-site magnetization consists of two parts (see Appendix B)

$$\Delta m^{(2)} = \Delta m_a^{(2)} + \Delta m_b^{(2)}, \quad (19)$$

where

$$\begin{aligned} \Delta m_a^{(2)} = & -\frac{64S}{N^3} \left(1 + \frac{r}{2S}\right) (1 - \kappa) \sum_{1-4} \frac{\Delta(1+2-3-4)}{(E_1 + E_2 + E_3 + E_4)^2} \\ & \times V^{(7)}(1234) V^{(8)}(3412) \left(\frac{1}{E_1} + \frac{1}{E_2} + \frac{1}{E_3} + \frac{1}{E_4} \right), \end{aligned} \quad (20)$$

$$\Delta m_b^{(2)} = \frac{16}{N^3} \sum_{1-4} \frac{\Delta(1+2-3-4)}{E_1 + E_2 + E_3 + E_4} W(1234), \quad (21)$$

$$\begin{aligned} W(1234) = & V^{(7)}(1234) \left[\frac{u_2^2 x_2^*}{E_2} V^{(5)}(3412) + \frac{u_3^2 x_3^*}{E_3} V^{(2)}(3412) \right] \\ & + V^{(8)}(3412) \left[\frac{u_1^2 x_1}{E_1} V^{(6)}(1234) + \frac{u_4^2 x_4}{E_4} V^{(3)}(1234) \right]. \end{aligned} \quad (22)$$

In the last equations the sums run over the vectors $\mathbf{k}_1, \mathbf{k}_2, \mathbf{k}_3, \mathbf{k}_4$ from the magnetic Brillouin zone; $\Delta(\mathbf{k})$ is the Kronecker function. The explicit expressions for the vertex functions $V^{(i)} \equiv V^{(i)}(\mathbf{k}_1, \mathbf{k}_2, \mathbf{k}_3, \mathbf{k}_4)$, $i = 1, \dots, 9$, are given in Appendix A. A straightforward task is to show that the above $6D$ integrals defining $\Delta E^{(2)}$ and $\Delta m^{(2)}$ are convergent, using the vertex expansions near $\mathbf{k} = 0$ and $\mathbf{k} = \pi^{13}$.

The $6D$ integrals written above were calculated using a standard Gaussian method for a set of lattices with up to $M = (20 \times 20)^3$ cells (each containing 4 points) and then the results were extrapolated to $M = \infty$. Starting from the $(4 \times 4)^3$ -cell lattice the results change monotonously and ensure the precision presented in Tables 1, 2.

III. COMPARISON WITH EXACT-DIAGONALIZATION DATA AND DISCUSSION

For the pure $J_1 = J_2$ Heisenberg model, the series for the ground-state energy E and on-site magnetization m read

$$E/2N = -0.33521 + 0.00019\lambda^2 + O(\lambda^3) = -0.33502 + O(\lambda^3), \quad (23)$$

$$m = 0.3034 + 0.0022\lambda^2 + O(\lambda^3) = 0.3056 + O(\lambda^3), \quad (24)$$

where $\lambda = 1$. The estimates for E and m are in accord with previous large- S ^{14,20} and numerical²¹ series results. The above series show that in the pure model the second-order $O(V_{DM}^2)$ corrections are numerically small (i.e., the effective quasiparticle interaction is weak) which means that the theory is self-consistent up to this order. As a matter of fact, the corrections $\Delta E^{(2)}$ do not exceed 3.5% of the MFT values in the whole range $-1.2 < \alpha < 5.0$ where the on-site magnetization m is positive. Notice that the second-order correction $\Delta E^{(2)}$ becomes negative²² for $\alpha < -0.8$ and $\alpha > 1.4$, Table 1. The second-order correction to the on-site magnetization $\Delta m^{(2)}$ is less than 10% as compared to m_0 in the interval $-0.9 < \alpha < 3.4$. $\Delta m^{(2)}$ is negative for $\alpha < -0.8$ and $\alpha > 1.6$, Table 2.

In Fig.3 we show the SWT results for the ground-state energy of Eq.(1) compared with ED data. The ED data are slightly size dependent, so that, for sake of clarity, we present only the results for a cluster with $N = 26$ spins. In the parameter range $-0.4 < \alpha < 2.0$ we find excellent agreement with ED data. Remember that $\alpha_s \approx 2.56$ is the numerical-series estimate for the order-disorder critical point⁶, and $\alpha = -1/3$ is the LSWT estimate for the second critical point of Eq.(1). For $\alpha > 2.0$ and $\alpha < -0.4$ one observes an increasing discrepancy with ED data. At the same time, the theory implies very small corrections to the zeroth-order energy E_0 in the whole range $-1.2 < \alpha < 4.0$. Analogous behavior of the SWT series has recently been indicated by Chubukov and Morr¹¹ in the two-layer Heisenberg antiferromagnet when approaching the quantum paramagnetic phase. It was argued, using an appropriate bosonization scheme²³, that the spin-wave description fails due to the enhanced longitudinal spin fluctuations near the quantum paramagnetic phase. Near the classical transition point $\alpha_c = -1/3$, where the melting of the Néel state is a result both of the frustration and zero-point spin fluctuations, the discussed discrepancy is less pronounced.

As a whole, the second-order correction to the on-site magnetization $\Delta m^{(2)}$, Fig. 4, improves the estimates for the helicoidal $\alpha_c \approx -1.2$ and paramagnetic $\alpha_s \approx 5.0$ critical points. However, the estimate for α_s is still twice larger than the numerical-series result $\alpha_s \approx 2.56$. At the same time, for instance at $\alpha = 2.5$, the correction $\Delta m^{(2)}$ is less than 3% from the mean-field value m_0 . In Fig. 4 we also present extrapolated ED data for the on-site magnetization deduced from the antiferromagnetic structure factor $M_s^2 = \frac{1}{N^2} \sum_{i,j} (-1)^{i+j} \langle \mathbf{S}_i \mathbf{S}_j \rangle$ using the cluster set $N = 16, 18, 20, 26$

and the extrapolation ansatz $M_s^2 = M_s^2(\infty) + \text{const}N^{-\frac{1}{2}}$. The ED estimate $m \approx 0.28$ at $\alpha = 1$ is smaller (but in agreement with other ED data using also the $N = 36$ cluster²⁴) than the SWT and numerical-series results mentioned above. The above discrepancy probably indicates the importance of the next-order term in the extrapolation ansatz²⁵. Notice that our ED estimate $\alpha_s \approx 2.4$ is in reasonable agreement with the numerical-series result $\alpha_s \approx 2.56$.

The SWT result $\alpha_c \approx -1.2$, Fig. 4, also exceeds the estimate obtained through an exact diagonalization of small clusters with $N = 16, 18, 20$ and 26 spins. The ED data predict a phase-transition point α_c which is close to the classical result $\alpha_c = -1/3$. Here the situation is analogous to the one in the $J_1 - J_2$ model containing frustrating diagonal bonds. For this model, both LSWT and the recent ED data^{24,26,27} predict a complete melting of the Néel phase at $J_2/J_1 \approx 0.4$, whereas an inclusion of the spin-wave interaction changes the estimate at least up to the classical transition point $J_2/J_1 = 0.5$ ^{16,28}. There is a smaller SWT estimate $J_2/J_1 \approx 0.43$ based on the standard large-S expansion²⁹, however it comes from large negative corrections $\Delta m^{(2)}$ reducing the effect of the diverging $\Delta m^{(1)}$ term, Eq.(4).

In conclusion, we have studied the influence of quantum spin fluctuations on the zero-temperature phase diagram of a $S = 1/2$ square-lattice Heisenberg antiferromagnet with two kinds of nearest-neighbor exchange bonds. The phase diagram is found to contain a helicoidal magnetic phase and a finite-gap quantum paramagnetic phase, both of them being separated through continuous transitions from the classical Néel phase. We constructed an appropriate spin-wave expansion and used exact-diagonalization data to find the changes of the phase diagram implied by the zero-point spin fluctuations. The latter approach reveals in particular the limits of the spin-wave description coming from the enhanced longitudinal spin fluctuations near the phase boundaries. The disagreement with ED data is strongly revealed in approaching the quantum-paramagnetic-phase boundary. In a forthcoming paper¹⁰ we present, in particular, ED-based analysis concerning the finite-gap quantum paramagnetic phase.

ACKNOWLEDGMENTS

N.I. was supported by the National Science Foundation, Grant $\Phi 412/94$. S.K. and J.R. were supported by DFG, Grant Ri-615/1-2. N.I. acknowledges the kind hospitality of the University at Magdeburg where part of this work was done. The visit in uni-Magdeburg was supported by DFG.

- ¹ For references concerning $J_1 - J_2$ and $J_1 - J_2 - J_3$ models, see A. V. Dotsenko and O. P. Sushkov, Phys. Rev. B **50**, 13821 (1994).
- ² T. Siegrist et al, Phys. Rev. B **35**, 7137 (1989); J. M. Tranquada, G. Shirane, B. Keimer, S. Shamoto, and M. Sato, Phys. Rev. B **40**, 4503 (1989); T. Matsuda and K. Hida, J. Phys. Soc. Jpn., **59** 2223 (1990); K. Hida, J. Phys. Soc. Jpn., **59** 2230 (1990); K. Hida, J. Phys. Soc. Japan, **61**, 1013 (1992); A. J. Millis and H. Monien, Phys. Rev. Lett., **70**, 2810 (1993); Phys. Rev. B **50**, 16606 (1994); A.W. Sandvik and D.J. Scalapino, Phys. Rev. Lett., **72**, 2777 (1994); A. V. Dotsenko, SISSA cond-mat/9505022 (1995); C. Gross, W. Wenzel, and J. Richter, preprint.
- ³ S. Chakravarty, B.I. Halperin, and D.R. Nelson, Phys. Rev. B **39**, 2344 (1989).
- ⁴ M. V. Feigelman and A. M. Tsvelik, Sov. Phys. JETP **49**, 1136 (1979); J. Vannimenus, S. Kirkpatrick, F. D. M. Haldane, and C. Jayaprakash, Phys. Rev. B **39**, 4634 (1988); Kong-Ju-Bock Lee and P. Schlottman, Phys. Rev. B **42**, 4426 (1990); D. D. Betts and J. Oitmaa, Phys. Rev. B **48**, 10602 (1993); J. Richter, Phys. Rev. B **47**, 5794 (1993); A. W. Sandvik, SISSA cond-mat/9407088 (1994); J. Oitmaa, D. D. Betts, and M. Aydin, Phys. Rev. B **51**, 2896 (1995); J. P. Rodriguez, J. Bonca, and J. Ferrer, Phys. Rev. B **51**, 3616 (1995); I. Ya. Korenblit, Phys. Rev. B **51**, (1995), in press.
- ⁵ A. Aharony, R. J. Birgeneau, A. Goniglio, M. A. Kastner, and H. E. Stanley, Phys. Rev. Lett. **60**, 1330 (1988).
- ⁶ R. R. P. Singh, M. P. Gelfand, and D. A. Huse, Phys. Rev. Lett. **61**, 2484 (1988).
- ⁷ L. B. Ioffe and A. I. Larkin, Int. J. Mod. Phys. B **2**, 203 (1988).
- ⁸ J. Ferrer, Phys. Rev. B **47**, 8769 (1993).
- ⁹ A. V. Chubukov, Phys. Rev. B **44**, 392 (1991).
- ¹⁰ In a forthcoming paper we present ED-data analysis of the discussed model, containing in particular estimates for the excitation gap in the quantum paramagnetic phase; J. Richter, S. E. Krüger, and N. B. Ivanov, to be published.
- ¹¹ A. V. Chubukov and D. K. Morr, SISSA cond-mat/9503029 (1995).
- ¹² E. Rastelli and A. Tassi, Phys. Rev. B **11**, 4711 (1975); E. Shendar, Zh. Eksp. Teor. Fiz. **83**, 326 (1982); A. Pimpinelli, E. Rastelli, and A. Tassi, J. Phys. Condens. Matter **1**, 2131 (1989).
- ¹³ P. Kopietz, Phys. Rev. B **41**, 9228 (1990).
- ¹⁴ C. M. Canali and M. Wallin, Phys. Rev. B **48**, 3264 (1993).

- ¹⁵ S. P. Obukhov, *Fiz. Tverd. Tela* **18**, 1098 (1976).
¹⁶ I. G. Gochev, *Phys. Rev. B* **49**, 9594 (1994).
¹⁷ T. Oguchi, *Phys. Rev.* **117**, 117 (1960).
¹⁸ J. Villain, R. Bidaux, J. P. Carton, and R. Conte, *J. Phys. Fr.* **41**, 1263 (1980).
¹⁹ C. M. Canali and S. M. Girvin, *Phys. Rev. B* **45**, 7127 (1992).
²⁰ C. J. Hamer, Z. Weihong, and P. Arndt, *Phys. Rev. B* **46**, 6276 (1992); J. Igarashi, *Phys. Rev. B* **46**, 10763 (1992); Z. Weihong and C. J. Hamer, *Phys. Rev. B* **47**, 7961 (1993).
²¹ R. R. P. Singh, *Phys. Rev. B* **39**, 9760 (1989); R. R. P. Singh, *Phys. Rev. B* **41**, 4873 (1990); Z. Weihong, J. Oitmaa, and C. J. Hamer, *Phys. Rev. B* **43**, 8321 (1991).
²² Notice that negative second-order corrections $\Delta E^{(2)}$ are possible only for non-Hermitian operators, such as the Dyson-Maleev interaction V_{DM} . Because the mean-field energy E_0 can also be regarded as a variational energy, one can speculate that the observed change of the sign indicates a kind of instability in the series.
²³ A. V. Chubukov and Th. Jolicoeur, *Phys. Rev. B* **44**, 12050 (1991).
²⁴ H. J. Schulz and T. A. L. Ziman, *Europhys. Lett.* **18**, 355 (1992); H. J. Schulz, T. A. Ziman, and D. Poilblanc, *SISSA cond-mat/9402061* (1994).
²⁵ We have also tried to extrapolate with quantum normalized M_s^2 , as it has recently been suggested by B. Bernu et al, *Phys. Rev. B* **50**, 10084 (1994), but the latter approach predicts for $\alpha = 1$ $m \approx 0.37$, which is less realistic.
²⁶ J. Richter, N. B. Ivanov, and K. Retzlaff, *J. Magn. Magn. Mat.* **140-144**, 1609 (1995).
²⁷ T. Einarsson and H. J. Schulz, *Phys. Rev. B* **51**, 6151 (1995).
²⁸ N. B. Ivanov and J. Richter, *J. Phys. Condens. Matter* **6**, 3785 (1994).
²⁹ J. Igarashi, *J. Phys. Soc. Jpn.*, **62** 4449 (1993).

APPENDIX A: DYSON-MALEEV VERTICES

The normal-ordered Dyson-Maleev interaction V_{DM} can be written in the following form¹⁹

$$\begin{aligned}
V_{DM} = & -\frac{2}{N} \sum_{1-4} \Delta(1+2-3-4) \\
& \times \left[V^{(1)} \alpha_1^\dagger \alpha_2^\dagger \alpha_3 \alpha_4 + V^{(2)} \alpha_1^\dagger \beta_2 \alpha_3 \alpha_4 + V^{(3)} \alpha_1^\dagger \alpha_2^\dagger \beta_3^\dagger \alpha_4 + V^{(4)} \alpha_1^\dagger \alpha_3 \beta_4^\dagger \beta_2 + V^{(5)} \beta_4^\dagger \alpha_3 \beta_2 \beta_1 \right. \\
& \left. + V^{(6)} \beta_4^\dagger \beta_3^\dagger \alpha_2^\dagger \beta_1 + V^{(7)} \alpha_1^\dagger \alpha_2^\dagger \beta_3^\dagger \beta_4^\dagger + V^{(8)} \beta_1 \beta_2 \alpha_3 \alpha_4 + V^{(9)} \beta_4^\dagger \beta_3^\dagger \beta_2 \beta_1 \right], \tag{A1}
\end{aligned}$$

where the sum runs over the vectors $\mathbf{k}_1, \mathbf{k}_2, \mathbf{k}_3, \mathbf{k}_4$ in the magnetic Brillouin zone and the Kronecker function $\Delta(\mathbf{k})$ expresses the conservation of momentum to within a reciprocal-lattice vector \mathbf{G} . For the Hamiltonian (1) the nine complex vertex functions are

$$\begin{aligned}
V^{(1)}(1234) = & \mathcal{U}(1234) \left(x_1 [x_4^* (\gamma_{1-4} - x_3^* \gamma_{1-3-4}) - (\gamma_1 - x_3^* \gamma_{1-3})] \right. \\
& \left. + x_2 [x_4^* (\gamma_{2-4} - x_3^* \gamma_{2-3-4}) - (\gamma_2 - x_3^* \gamma_{2-3})] \right), \tag{A2}
\end{aligned}$$

$$\begin{aligned}
V^{(2)}(1234) = & 2\mathcal{U}(1234) \left(x_1 x_2^* [x_4^* (x_3^* \gamma_{1-3-4} - \gamma_{1-4}) - (x_3^* \gamma_{1-3} - \gamma_1)] \right. \\
& \left. + [x_4^* (x_3^* \gamma_{2-3-4} - \gamma_{2-4}) - (x_3^* \gamma_{2-3} - \gamma_2)] \right), \tag{A3}
\end{aligned}$$

$$\begin{aligned}
V^{(3)}(1234) = & 2\mathcal{U}(1234) \left(x_1 [x_4^* (\gamma_{1-3-4} - x_3 \gamma_{1-4}) - (\gamma_{1-3} - x_3 \gamma_1)] \right. \\
& \left. + x_2 [x_4^* (\gamma_{2-3-4} - x_3 \gamma_{2-4}) - (\gamma_{2-3} - x_3 \gamma_2)] \right), \tag{A4}
\end{aligned}$$

$$\begin{aligned}
V^{(4)}(1234) = & 4\mathcal{U}(1234) \left(x_1 x_2^* [x_4 (x_3^* \gamma_{1-3} - \gamma_1) - (x_3^* \gamma_{1-3-4} - \gamma_{1-4})] \right. \\
& \left. + [x_4 (x_3^* \gamma_{2-4} - \gamma_2) - (x_3^* \gamma_{2-3-4} - \gamma_{2-4})] \right), \tag{A5}
\end{aligned}$$

$$\begin{aligned}
V^{(5)}(1234) = & 2\mathcal{U}(1234) \left(x_2^* [(x_3^* \gamma_{1-3-4} - \gamma_{1-4}) - x_4 (x_3^* \gamma_{1-3} - \gamma_1)] \right. \\
& \left. + x_1^* [(x_3^* \gamma_{2-3-4} - \gamma_{2-4}) - x_4 (x_3^* \gamma_{2-3} - \gamma_2)] \right), \tag{A6}
\end{aligned}$$

$$V^{(6)}(1234) = 2\mathcal{U}(1234) \left(x_1^* x_2 [x_4 (x_3 \gamma_2 - \gamma_{2-3}) - (x_3 \gamma_{2-4} - \gamma_{2-3-4})] \right)$$

$$+ [x_4(x_3\gamma_1 - \gamma_{1-3}) - (x_3\gamma_{1-4} - \gamma_{1-3-4})]), \quad (\text{A7})$$

$$V^{(7)}(1234) = \mathcal{U}(1234) \left(x_1 [x_4(\gamma_{1-3} - x_3\gamma_1) - (\gamma_{1-3-4} - x_3\gamma_{1-4})] \right. \\ \left. + x_2 [x_4(\gamma_{2-3} - x_3\gamma_2) - (\gamma_{2-3-4} - x_3\gamma_{2-4})] \right), \quad (\text{A8})$$

$$V^{(8)}(1234) = \mathcal{U}(1234) \left(x_2^* [(x_3^*\gamma_{1-3} - \gamma_1) - x_4^*(x_3^*\gamma_{1-3-4} - \gamma_{1-4})] \right. \\ \left. + x_1^* [(x_3^*\gamma_{2-3} - \gamma_2) - x_4^*(x_3^*\gamma_{2-3-4} - \gamma_{2-4})] \right), \quad (\text{A9})$$

$$V^{(9)}(1234) = \mathcal{U}(1234) \left(x_2^* [x_4(\gamma_{1-3} - x_3\gamma_1) - (\gamma_{1-3-4} - x_3\gamma_{1-4})] \right. \\ \left. + x_1^* [x_4(\gamma_{2-3} - x_3\gamma_2) - (\gamma_{2-3-4} - x_3\gamma_{2-4})] \right), \quad (\text{A10})$$

where $\mathcal{U}(1234) \equiv u_1 u_2 u_3 u_4$ and the Bogoliubov coefficients $u_{\mathbf{k}}$ and $x_{\mathbf{k}} \equiv -v_{\mathbf{k}}/u_{\mathbf{k}}$ are dedined by Eq.(14). $\gamma_{\mathbf{k}}$ is a complex lattice structure factor given by

$$\gamma_{\mathbf{k}} = \nu_{\mathbf{k}} - \kappa_0 \cos k_x + i\kappa_0 \sin k_x, \quad (\text{A11})$$

where $\nu_{\mathbf{k}} = (\cos k_x + \cos k_y)/2$, $\kappa_0 \equiv (1 - \alpha)/4$. In the symmetric $J_1 = J_2$ model, the vertex functions are real and reduce to the well-known Dyson-Maleev vertices¹⁹.

APPENDIX B: CALCULATION OF $\Delta M^{(2)}$

A straightforward way to find the second-order correction to on-site magnetization $\Delta m^{(2)}$ is to introduce in H a perturbing staggered magnetic field h (see, e.g., Ref. 16). The perturbed Hamiltonian reads

$$H(h) = H - hN\hat{m} \equiv E_0(h) + H_0(h) + V_{DM}, \quad (\text{B1})$$

where the on-site magnetization operator has the form

$$\hat{m} = S - \frac{2}{N} \sum_{\mathbf{k}} |v_{\mathbf{k}}|^2 - \frac{1 - \kappa}{N} \sum_{\mathbf{k}} \frac{1}{\varepsilon_{\mathbf{k}}} \left[(\alpha_{\mathbf{k}}^\dagger \alpha_{\mathbf{k}} + \beta_{\mathbf{k}}^\dagger \beta_{\mathbf{k}}) - 2u_{\mathbf{k}}^2 (x_{\mathbf{k}} \alpha_{\mathbf{k}}^\dagger \beta_{\mathbf{k}}^\dagger + h.c.) \right]. \quad (\text{B2})$$

In the new basis of $H_0(h)$ the second-order correction to the ground-state energy reads

$$\Delta E^{(2)}(h) = - \sum_{[\rho_h]} \frac{\langle 0_h | V_{DM} | \rho_h \rangle \langle \rho_h | V_{DM} | 0_h \rangle}{E_{\rho_h}}, \quad (\text{B3})$$

where $|\rho_h \rangle$ are four-particle eigenstates of $H_0(h)$.

$\Delta m^{(2)}$ can be obtained by applying the Hellmann-Feynman theorem to Eq.(B1) and then using Eq.(B3)

$$\Delta m^{(2)} = -\frac{1}{N} \frac{\partial}{\partial h} \Delta E^{(2)}(h)_{h=0}. \quad (\text{B4})$$

There are two contributions to Eq.(B4) $\Delta m_a^{(2)}$ and $\Delta m_b^{(2)}$, coming respectively from the $O(h)$ terms in the dominator and numerator of Eq.(B3). A simple calculation using

$$E_{\mathbf{k}}(h) = E_{\mathbf{k}} + (1 - \kappa) \frac{h}{\varepsilon_{\mathbf{k}}} + O(h^2), \quad (\text{B5})$$

gives the correction $\Delta m_a^{(2)}$, Eq.(20).

The second contribution $\Delta m_b^{(2)}$ results from the $O(h)$ corrections in the numerator of Eq.(B3). It is easy to check that the field corrections to the four-particle states $|\rho \rangle$ do not contribute up to the required $O(h)$ order, so that it is enough to put in Eq.(B3) the unperturbed state $|\rho \rangle$, and to use the following expression for the perturbed ground state $|0_h \rangle$

$$|0_h \rangle = |0 \rangle - 2h \sum_{\mathbf{k}} \frac{u_{\mathbf{k}}^2 x_{\mathbf{k}}}{-2E_{\mathbf{k}}} |\mathbf{k} \rangle + O(h^2). \quad (\text{B6})$$

Here $|\mathbf{k} \rangle = \alpha_{\mathbf{k}}^\dagger \beta_{\mathbf{k}}^\dagger |0 \rangle$. Then a straightforward calculation of the respective matrix elements yields Eq.(21) for $\Delta m_b^{(2)}$.

FIG. 1. The classical helicoidal state in a square-lattice Heisenberg antiferromagnet with two kinds of regularly distributed nearest-neighbor exchange bonds, J_1 and J_2 . The helicoidal phase is stable for $\alpha \equiv J_2/J_1 < -1/3$. The spin orientations at A and B lattice sites are defined by the angles $\theta_n = n\Phi$ and $\theta_n = n\Phi + \pi$, respectively, where $n = 0, 1, 2, \dots$. The state is shown for $\Phi = \pi/12$, i.e., $\alpha = -1/(1 + \sqrt{3})$, and $n = 0, 1, \dots, 7$.

FIG. 2. Phase diagram of the $S = 1/2$ system in a linear spin-wave approximation (LSWT). The solid lines represent the on-site magnetization m as a function of the parameter $\alpha \equiv J_2/J_1$. The dashed line shows the diverging first-order correction. There is a small region around the classical transition point $\alpha_c = -1/3$ ($-0.336 < \alpha < -0.331$) where the magnetic states are melt. For $\alpha > \alpha_s$ a finite-gap quantum paramagnetic phase is stable. $\alpha_s \approx 10.6$ in LSWT.

FIG. 3. Ground-state energy of the model vs $\alpha \equiv J_2/J_1$, $S = 1/2$. The open circles are ED data for $N = 26$. ED data for $N = 16, 18, 20$ are not shown but the deviations from the $N = 26$ cluster are very small. E_0 is the zeroth-order mean-field result.

FIG. 4. On-site magnetization in the Néel phase vs $\alpha \equiv J_2/J_1$ calculated up to second order in V_{DM} , $S = 1/2$. m_0 is the zeroth-order mean-field result and $\Delta m^{(2)}$ is the second-order $O(V_{DM}^2)$ correction. The stars represent extrapolated ED data for the on-site magnetization deduced from the antiferromagnetic structure factor $M_s^2 = \frac{1}{N^2} \sum_{i,j} (-1)^{i+j} \langle \mathbf{S}_i \mathbf{S}_j \rangle$ using the cluster set $N = 16, 18, 20, 26$ and the extrapolation ansatz $M_s^2 = M_s^2(\infty) + \text{const}N^{-\frac{1}{2}}$

TABLE I. Data for the ground-state energy E of the Néel phase calculated up to second-order corrections $\Delta E^{(2)}$ in respect to V_{DM} . $\alpha = J_2/J_1$, $E = E_0 + \Delta E^{(2)}$. E_0 is the zeroth-order mean-field energy. $S = 1/2$.

α	$E_0/2N$	$\Delta E^{(2)}/2N$	$E/2N$	α	$E_0/2N$	$\Delta E^{(2)}/2N$	$E/2N$
-2.0	-0.21563	-0.036	-0.252	0.4	-0.29085	0.00005	-0.29080
-1.8	-0.21811	-0.023	-0.241	0.6	-0.30429	0.00009	-0.30420
-1.6	-0.22094	-0.014	-0.235	0.8	-0.31909	0.00015	-0.31894
-1.4	-0.22421	-0.0078	-0.2320	1.0	-0.33521	0.00019	-0.33502
-1.3	-0.22604	-0.0054	-0.2315	1.2	-0.35259	0.00016	-0.35243
-1.2	-0.22800	-0.0035	-0.2315	1.4	-0.37117	0.00006	-0.37111
-1.1	-0.23012	-0.0021	-0.2322	1.6	-0.39089	-0.00015	-0.39104
-1.0	-0.23241	-0.0010	-0.2334	1.8	-0.41168	-0.00046	-0.41214
-0.8	-0.23755	0.0002	-0.2374	2.0	-0.43348	-0.00088	-0.43436
-0.6	-0.24356	0.0006	-0.2430	2.4	-0.47987	-0.00206	-0.48193
-0.4	-0.25056	0.0006	-0.2500	2.8	-0.52964	-0.00372	-0.53336
-0.2	-0.25870	0.00037	-0.25833	3.6	-0.63800	-0.00852	-0.64652
0.0	-0.26808	0.00017	-0.26791	4.0	-0.69606	-0.01173	-0.70779
0.2	-0.27878	0.00006	-0.27872				

TABLE II. Data for the on-site magnetization m of the Néel phase calculated up to second-order corrections $\Delta m^{(2)}$ in respect to V_{DM} . $\alpha = J_2/J_1$, $m = m_0 + \Delta m^{(2)}$. m_0 is the zeroth-order on-site magnetization. $S = 1/2$.

α	m_0	$\Delta m^{(2)}$	m	α	m_0	$\Delta m^{(2)}$	m
-1.2	0.1726	-0.14	0.03	1.4	0.2996	0.0016	0.3012
-1.1	0.1819	-0.08	0.10	1.6	0.2952	0.0009	0.2961
-1.0	0.1911	-0.04	0.15	1.8	0.2894	-0.0002	0.2892
-0.8	0.2095	0.001	0.211	2.0	0.2824	-0.0016	0.2808
-0.6	0.2274	0.012	0.239	2.2	0.2743	-0.0034	0.2709
-0.4	0.2444	0.0112	0.2556	2.4	0.2652	-0.0054	0.2598
-0.2	0.2599	0.0075	0.2674	2.6	0.2553	-0.008	0.247
0.0	0.2734	0.0044	0.2778	2.8	0.2446	-0.010	0.235
0.2	0.2846	0.0026	0.2872	3.0	0.2331	-0.014	0.219
0.4	0.2931	0.0019	0.2950	3.2	0.2210	-0.017	0.204
0.6	0.2990	0.0019	0.3009	3.4	0.2081	-0.021	0.187
0.8	0.3024	0.0021	0.3045	3.6	0.1946	-0.025	0.170
1.0	0.3034	0.0022	0.3056	3.8	0.1805	-0.030	0.150
1.2	0.3024	0.0020	0.3044	4.0	0.1657	-0.036	0.130

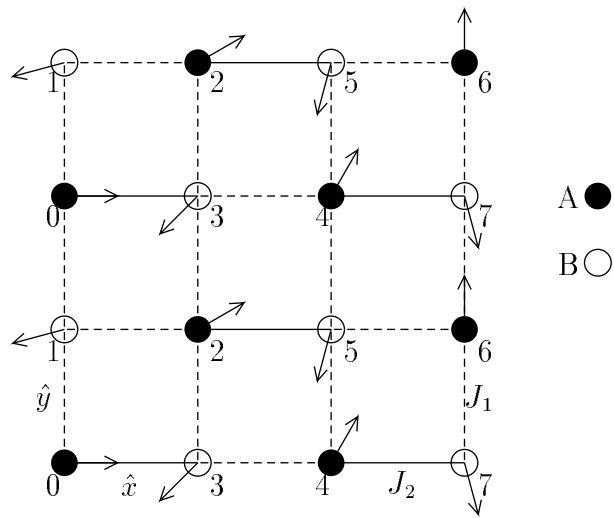


Fig. 1

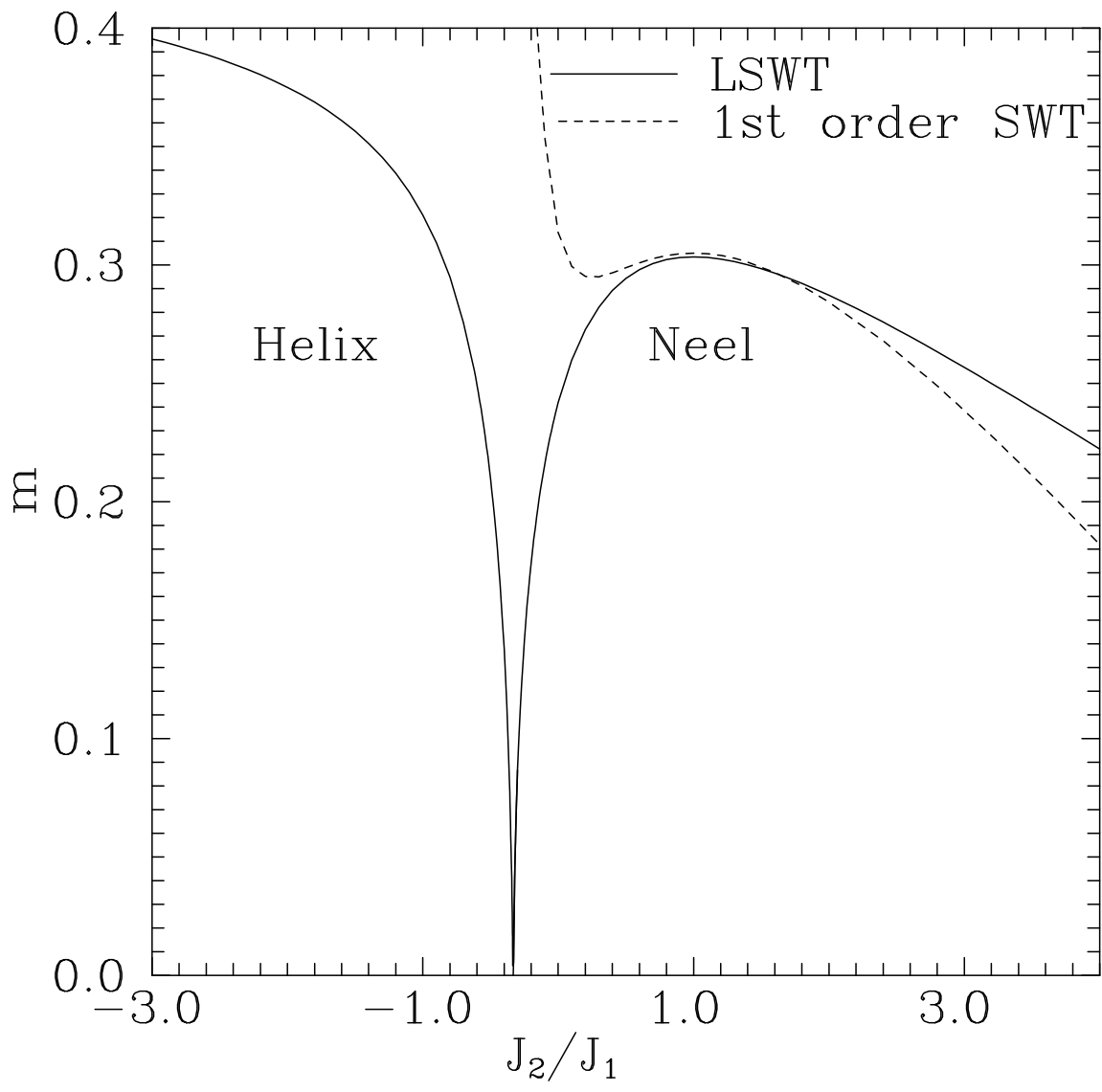


Fig. 2

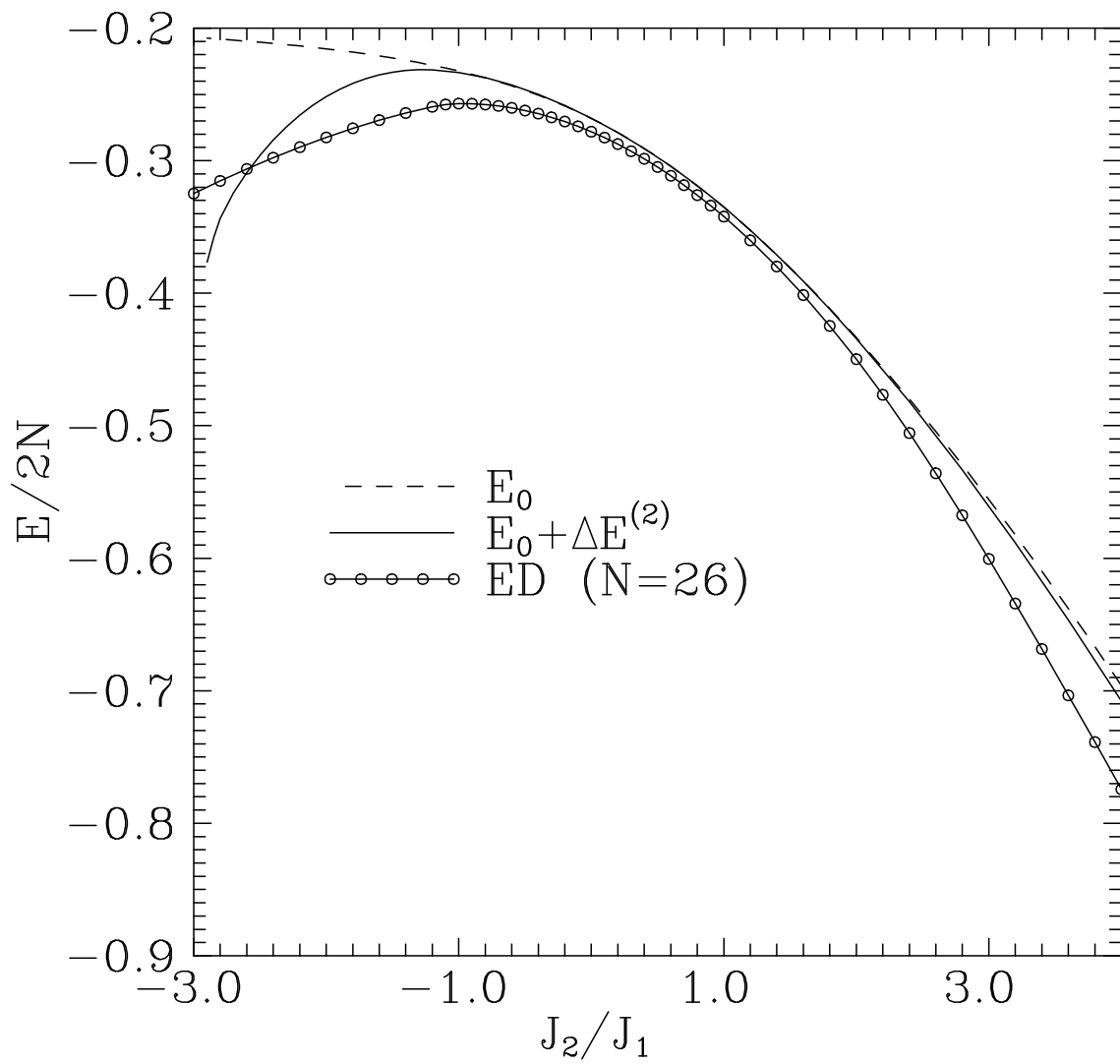


Fig. 3

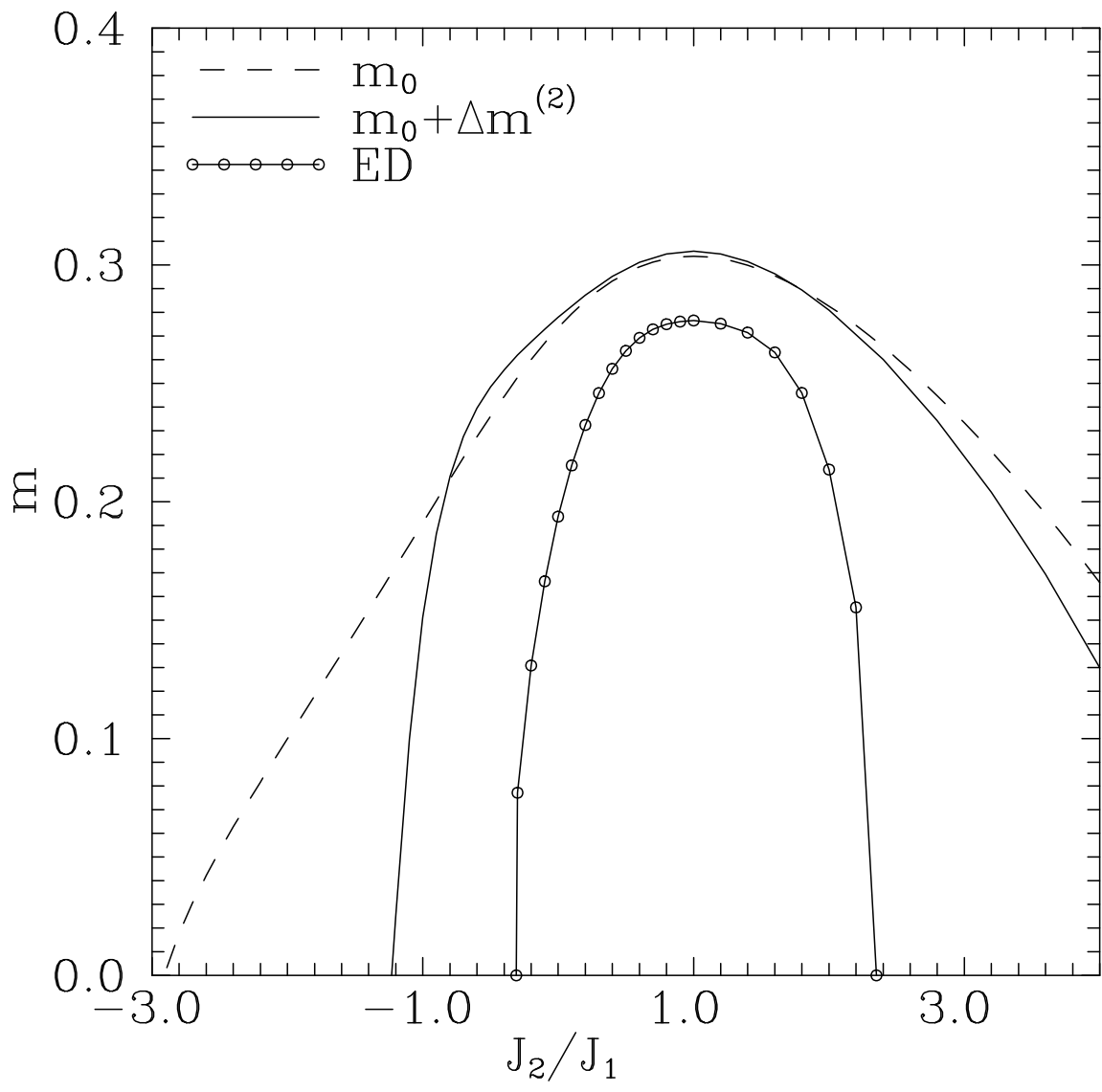


Fig. 4